Monitoring Needle Biopsy of Sentinel Lymph Nodes Using Photoacoustic Image with Dynamic-FDMAS Beamformer

Abdulrhman Alshaya*†, Luzhen Nie*, David M. J. Cowell*, T. Carpenter*, James R. McLaughlan*‡, and Steven Freear*

*Ultrasonics and Instrumentation Group, School of Electronic and Electrical Engineering, University of Leeds, Leeds, LS2 9JT, U.K.

†King Abdulaziz City for Science and Technology (KACST), Riyadh, Saudi Arabia

‡Leeds Institute of Cancer and Pathology, School of Medicine, University of Leeds, Leeds, LS9 7TF, U.K.

E-mail: aaalshaya@kacst.edu.sa and S.Freear@leeds.ac.uk

***Abstract*—As a part of the diagnosis pathway for breast cancer, a needle biopsy of the sentinel lymph node (SLN) is taken for analysis. Photoacoustic imaging is a better approach for guiding a needle than ultrasound imaging. However, the photoacoustic image will be affected by clutter, phase aberration and artefact from the needle. In this study, a dynamic filter delay multiply and sum (D-FDMAS) beamformer was produced to reduce these effects and improve the SNR and contrast difference (CD) of imaging targets. The D-FDMAS beamformer with a sub-group of 16 elements (16 D-FDMAS) showed improvement in SNR of needle and inclusion (SLN) by 8.38 dB and 5.42 dB compared with the delay and sum (DAS) beamfomer. It also showed reduction in CD between the inclusion and needle by almost 12 dB compared with the filter delay multiply and sum (FDMAS) beamformer.**

I. Introduction

Breast cancer is one of the common cancers that women suffer from. It is a reason of death more than 0.5 million women in 2012 [1], [2]. An early detection of breast cancer will lead to increase the percentage of the survive rate [3], [4]. As a part of the diagnosis pathway for breast cancer, a needle biopsy of the sentinel lymph node (SLN) is taken for analysis. When ultrasound imaging is used, it will be difficult to differentiate between the SLN and other lymph nodes [5]. Therefore, researchers investigate photoacoustic imaging to guide the needle. In photoacoustic imaging, exogenous contrast agents such as indocyanine green (ICG) are injected near the tumour. This contrast agent that has a narrow optical absorption spectrum propagates through the lymphatic system. As a result, the location of the SLN is defined by generating photoacoustic images of these agent [5], [6].

In photoacoustic imaging, clutter, phase aberration and directivity of the transducer affect the image equality. These effects are high when the most popular delay and sum (DAS) beamformer is used. In this beamformer, the spatial resolution is reduced and side-lobes and artefact are generated [7]–[9]. Researchers have used some advanced beamforming techniques such as the filter delay multiply and sum (FDMAS) beamformer, to reduce these effect [10], [11]. This beamfoerming technique shows improvement in spatial resolution and reduction in side-lobes. However, the correlation operation in the FDMAS beamformer affects the contrast difference (CD) between different targets such as the SLN and needle.

In this study, the dynamic filter delay multiply and sum (D-FDMAS) beamformer was produced to reduce these effects and improve signal to noise ratio (SNR), spatial resolution and contrast of the photoacoustic image. The D-FDMAS beamformer will be compared with DAS and FDMAS beamformers in terms of SNR and CD based on needle experiments.

II. Method

A. Dynamic Filter Delay Multiply and Sum (D-FDMAS) Beamforming technique

The D-FDMAS beamformer depends on the correlation operation between a delayed RF-signal of sub-group of transducer elements. This is unlike the FDMAS beamformer that depends on the correlation operation between the delayed RF-signals from all transducer elements. The ideal of D-FDMAS is taken from the sub-FDMAS beamformer [11]. However, In the D-FDMAS beamformer, the delayed RF-signal for each transducer element is correlated with itself to emphasize the energy of the beamformed data as given in Eq.1:

$$y_{D-FDMAS} = \{\sum_{i=1}^{N}\sum_{j=i}^{m} sign(S_i(t)S_j(t)).\sqrt{|S_i(t)S_j(t)|}\} * f,$$

$$m = \begin{cases} i+L-1 & L \leq N-i \\ N & else \end{cases}, \tag{1}$$

where N is the number of transducer elements, $S_i(t)$ and $S_j(t)$ are the delayed RF-signals for element i and j, respectively, L is the sub-group size, $sign$ is the sign operation to save the signal phase after multiplication and f is a band pass filter to remove the low-frequency part of the signal. In this beamformer, the delayed RF-signal for each transducer element is correlated with itself to emphasize the energy of the beamformed data that have been applied before by Su *et al.* [12]. The number of multiplication operations when using the D-FDMAS beamformer is calculated by using Eq.2:

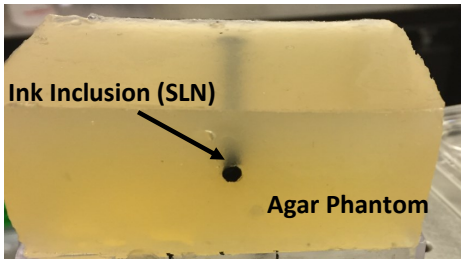

Fig. 1: The agar phantom with ink inclusion to imitate a SLN.

$$NU_{D-FDMAS} = LN - (\frac{L^2 - L}{2}), \tag{2}$$

III. Experiment Setup

An agar phantom with an inclusion as shown in Fig. 1 was used in the experiment. The recipe of the agar phantom was taken from [13], [14]. The same recipe was used for the inclusion excipt the agar material was not used and 20 % Indian ink (Dr.Ph.Martins, Black Star) was used as the absorbent material. This inclusion was used to simulate a SLN. The depth of this inclusion was around 1.2 cm. A needle (Blunt Fill Needle, 18G) was inserted inside the phantom to generate photoacoustic emissions from the needle and inclusion simultaneously. The setup of this experiment is shown in Fig. 2. The Nd-YAG laser was used to fire laser pulses on the phantom. These pulses were guided to the phantom through an optical fibre that had one input and seven outputs (BF76LS01, Thorlabs). The wavelenght and the energy per pulse were 850 nm and 3.7 mJ, respectively. The generated photoacoustic emissions were recorded by using the Ultrasound Array Research Platform II (UARP II) [15]–[18] with a 128-element linear transducer (Verasonics L11-4). The center frequency and bandwidth (- 6 dB) of the linear transducer were 7 MHz and (4 to 11) MHz, respectively. These received photoacoustic emissions were averaged 100 times before beamforming. The data was analysed based on SNR and CD after beamforming with the DAS, FDMAS and D-FDMAS beamformers.

IV. Results and Discussion

The received photoacoustic emissions were beamformed by using D-FDMAS with different sub-group sizes as shown in Fig. 3. The background noise and needle artefact were reduced as the sub-group size was increased. However, the CD between the needle and inclusion was increased when the sub-group size was increased. The SNR and CD of the inclusion and needle were calculated for different sub-group sizes. The SNR was calculated by using Eq. 3 [19]:

$$SNR = 20\log_{10}(\frac{\mu_{Signal}}{\sigma_{Backgound}}), \tag{3}$$

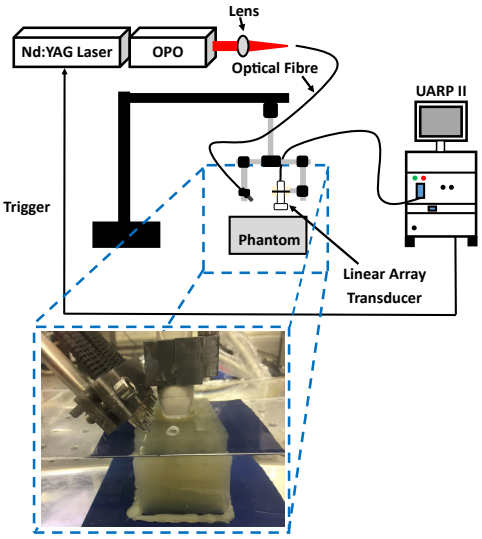

Fig. 2: The experimental setup.

where μ_{Signal} is the mean of the signal and $\sigma_{Backgound}$ is the standard deviation of the background. In Fig. 3 (A), the solid rectangle number 1 and 2 delineate the signal and background noise regions, respectively, for the needle. The dashed rectangle number 1 and 2 show the signal and background noise regions, respectively, for the inclusion. Table. I shows the SNR of photoacoustic images beamformed by using D-FDMAS with different sub-group sizes. The contrast ratio (CR) was calculated by using Eq. 4 [20]:

$$CR = 20\log_{10}(\frac{\mu_{Signal}}{\mu_{Backgound}}), \tag{4}$$

where $\mu_{Backgound}$ is the mean of the background. In Fig. 3 (A), the solid rectangle number 1 and the dashed rectangle number 1 are the signal regions of needle and inclusion, respectively. The solid rectangle number 2 is the background region. Table. II shows the CD between the needle and inclusion when photoacoustic images beamformed by using D-FDMAS with different sub-group sizes. From Table. I and Table. II, The highest SNR for the needle was 26.29 dB when the sub-group had 16 elements. The SNR of the inclusion was improved as the sub-group size was increased. However, the CD between the inclusion and needle was increased as the sub-group size was increased. For instance, when the sub-group occupied 4 elements, the CD was 0.52 dB. This CD was increased to 13.78 dB when the sub-group had 128 elements. By using 16 D-FDMAS and 32 D-FDMAS, the CD was 2.23 dB and 7.89 dB, respectively. These CD do not effect recognizing inclusion and needle as shown in Figs. 3 (C) and (D).

The 16 D-FDMAS beamformer was compared with the DAS and FDMAS beamformers as shown in Fig. 4. Fig. 4 (A) shows the ultrasound image for the inclusion and needle. This ultrasound image was generated from a single plane wave. The contrast of the needle was low. Fig. 4 (B) shows the photoacoustic image for the needle and inclusion when the

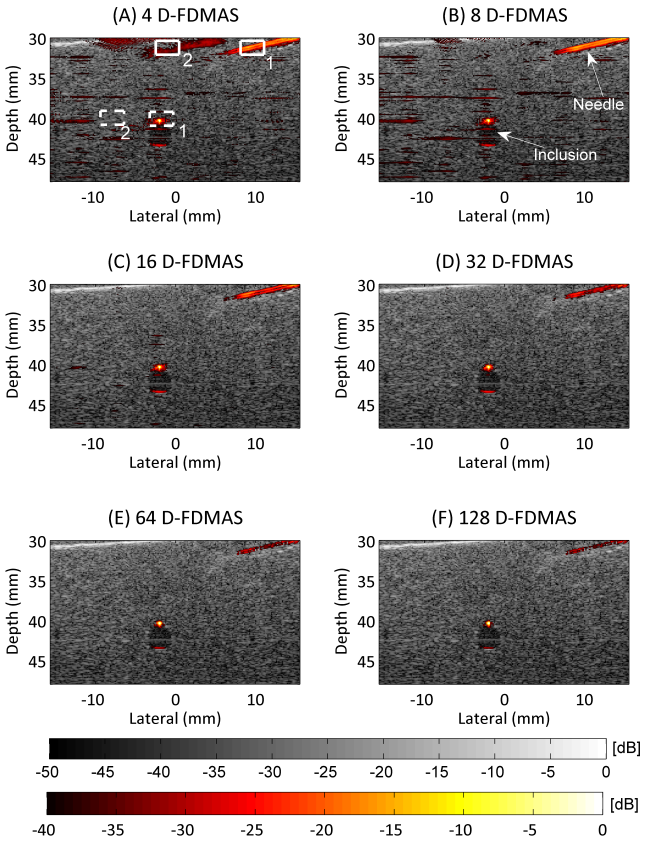

Fig. 3: Photoacoustic images of the inclusion and needle when the D-FDMAS beamformer with different sub-group sizes were used. (A) 4 elements, (B) 8 elements, (C) 16 elements, (D) 32 elements, (E) 64 elements and (F) 128 elements. In all photoacoustic images (Hot colormap), the ultrasound image (Gray colormap) was used as the background. The dynamic range of ultrasound and photoacoustic images are 50 dB and 40 dB, respectively.

TABLE I: SNR of the photoacoustic images beamformed by using D-FDMAS with different sub-group sizes.

D-FDMAS	**SNR (dB)**	
Sub-group	**Inclusion**	**Needle**
4	25.86	21.14
8	27.52	25.4
16	32.17	26.29
32	36.03	21.71
64	42.04	21.05
128	43.47	21.13

DAS beamformer was used. In this photoacoustic image, the background noise is high. There are also high-level artefact from the needle. When the FDMAS beamformer was used as shown in Fig. 4 (C), the background noise and needle artefacts are significantly reduced. However, the CD between the needle and inclusion was increased. This will negatively affect the recognition of the needle. This is because the difference shape of the propagation RF-signals between needle and inclusion. The SNR and CD of the inclusion and needle were calculated by using the same step that is used with the D-FDMAS beamformer. Table. III and Table. IV show the SNR and CD when using DAS, FDMAS and 16 D-FDMAS. From Table. III and Table. IV, the FDMAS beamformer improved the SNR of the needle and inclusion by 3 dB and 17.44 dB, respectively, when compared with the DAS beamformer. However, the CD between the needle and inclusion was increased by almost 13 dB. This creates difficulties to recognize and track the needle as shown in Fig. 4 (C). The 16 D-FDMAS beamformer (Fig. 4 (D)) improved the SNR of the inclusion and needle by 5.42 dB and 8.38 dB, respectively, when compared with the DAS beamformer. In addition, it reduced the CD by almost 12 dB compared with the FDMAS beamformer.

TABLE II: CR of photoacoustic image beamformed by using D-FDMAS with different sub-group size.

D-FDMAS	**Contrast Ratio (dB)**		
Sub-group	**Inclusion**	**Needle**	**Difference**
4	15.01	15.53	0.52
8	17.79	18.79	1.00
16	22.41	20.18	2.23
32	26.11	18.23	7.89
64	30.27	17.74	12.52
128	31.52	17.74	13.78

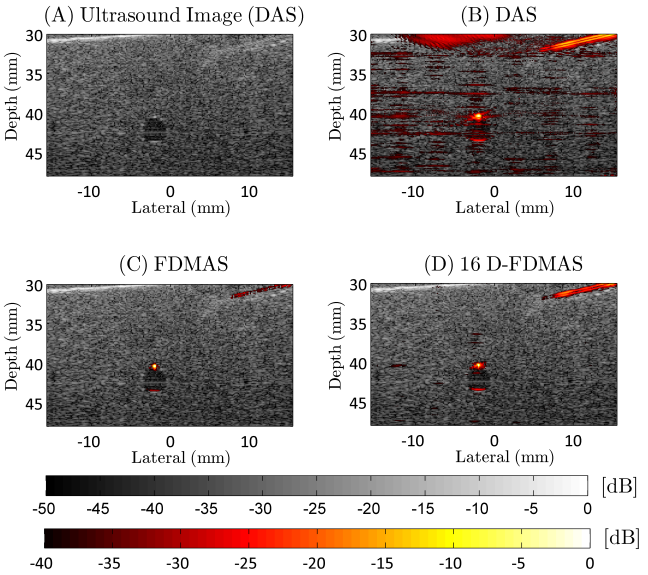

Fig. 4: Ultrasound and photoacoustic images of the inclusion and needle. (A) Ultrasound image, (B) photoacoustic image with DAS, (C) photoacoustic image with FDMAS and (D) photoacoustic image with 16 D-FDMAS. In all photoacoustic images, the ultrasound image was used as the background. The dynamic range of ultrasound and photoacoustic images are 50 dB and 40 dB, respectively.

TABLE III: SNR of the photoacoustic images.

	SNR (dB)	
Beamformer	**Inclusion**	**Needle**
DAS	26.75	17.91
FDMAS	44.19	20.95
16 D-FDMAS	32.17	26.29

TABLE IV: CR of the photoacoustic images.

	Contrast Ratio (dB)		
Beamformer	**Inclusion**	**Needle**	**Difference**
DAS	10.82	9.85	0.97
FDMAS	31.53	17.41	14.12
16 D-FDMAS	22.41	20.18	2.23

The number of multiplications when using D-FDMAS depends on the sub-group size. When the number of transducer elements is 128, there should be 16 to 32 elements in each sub-group. From Eq. 2, when the sub-group size is 32 elements, the number of multiplications is 3600. Whereas when the FDMAS beamformer is used, the number of multiplications is 8128. The lower computational cost could make the D-FDMAS beamformer more suitable for real time imaging when it is processed by using a GPU.

V. Conclusion

In this paper, the D-FDMAS beamformer was used to co-locate needle and inclusion (SLN). The optimum sub-group size was between 16 and 32 elements. By using D-FDMAS with 16 elements in a sub-group, the CD was significantly reduced compared with the FDMAS beamformer. The SNR of the needle and inclusion was enhanced by 8.38 dB and 5.42 dB, respectively, when compared with the DAS beamformer. In addition, the computation time of the D-FDMAS beamfomer is much less than that of the FDMAS beamfomer.

References

[1] M. I. Nounou, F. ElAmrawy, N. Ahmed, K. Abdelraouf, S. Goda, and H. Syed-Sha-Qhattal, "Breast cancer: conventional diagnosis and treatment modalities and recent patents and technologies," *Breast cancer: basic and clinical research*, vol. 9, pp. BCBCR–S29 420, 2015.

[2] M. Heijblom, D. Piras, M. Brinkhuis, J. C. van Hespen, F. Van den Engh, M. Van der Schaaf, J. Klaase, T. Van Leeuwen, W. Steenbergen, and S. Manohar, "Photoacoustic image patterns of breast carcinoma and comparisons with magnetic resonance imaging and vascular stained histopathology," *Scientific reports*, vol. 5, p. 11778, 2015.

[3] S. Zackrisson, S. Van De Ven, and S. Gambhir, "Light in and sound out: emerging translational strategies for photoacoustic imaging," *Cancer research*, vol. 74, no. 4, pp. 979–1004, 2014.

[4] M. Mehrmohammadi, S. Joon Yoon, D. Yeager, and S. Y Emelianov, "Photoacoustic imaging for cancer detection and staging," *Current molecular imaging*, vol. 2, no. 1, pp. 89–105, 2013.

[5] K. Sivasubramanian, V. Periyasamy, and M. Pramanik, "Non-invasive sentinel lymph node mapping and needle guidance using clinical handheld photoacoustic imaging system in small animal," *Journal of biophotonics*, vol. 11, no. 1, p. e201700061, 2018.

[6] C. Kim, T. N. Erpelding, K. I. Maslov, L. Jankovic, W. J. Akers, L. Song, S. Achilefu, J. A. Margenthaler, M. D. Pashley, and L. V. Wang, "Handheld array-based photoacoustic probe for guiding needle biopsy of sentinel lymph nodes," *Journal of biomedical optics*, vol. 15, no. 4, p. 046010, 2010.

[7] E. J. Alles, M. Jaeger, and J. C. Bamber, "Photoacoustic clutter reduction using short-lag spatial coherence weighted imaging," in *Ultrasonics Symposium (IUS), 2014 IEEE International*. IEEE, 2014, pp. 41–44.

[8] S. Park, S. Mallidi, A. B. Karpiouk, S. Aglyamov, and S. Y. Emelianov, "Photoacoustic imaging using array transducer," in *Photons Plus Ultrasound: Imaging and Sensing 2007: The Eighth Conference on Biomedical Thermoacoustics, Optoacoustics, and Acousto-optics*, vol. 6437. International Society for Optics and Photonics, 2007, p. 643714.

[9] S. Park, A. B. Karpiouk, S. R. Aglyamov, and S. Y. Emelianov, "Adaptive beamforming for photoacoustic imaging," *Optics letters*, vol. 33, no. 12, pp. 1291–1293, 2008.

[10] G. Matrone, A. S. Savoia, G. Caliano, and G. Magenes, "The delay multiply and sum beamforming algorithm in ultrasound b-mode medical imaging," *IEEE transactions on medical imaging*, vol. 34, no. 4, pp. 940–949, 2015.

[11] A. Alshaya, S. Harput, A. M. Moubark, D. M. J. Cowell, J. McLaughlan, and S. Freear, "Spatial resolution and contrast enhancement in photoacoustic imaging with filter delay multiply and sum beamforming technique," in *2016 IEEE International Ultrasonics Symposium (IUS)*, Sept 2016, pp. 1–4.

[12] T. Su, D. Li, and S. Zhang, "An efficient subarray average delay multiply and sum beamformer algorithm in ultrasound imaging," *Ultrasonics*, vol. 84, pp. 411–420, 2018.

[13] L. Nie, S. Harput, D. M. J. Cowell, T. M. Carpenter, J. R. Mclaughlan, and S. Freear, "Combining acoustic trapping with plane wave imaging for localized microbubble accumulation in large vessels," *IEEE Transactions on Ultrasonics, Ferroelectrics, and Frequency Control*, vol. 65, no. 7, pp. 1193–1204, July 2018.

[14] J. Browne, K. Ramnarine, A. Watson, and P. Hoskins, "Assessment of the acoustic properties of common tissue-mimicking test phantoms," *Ultrasound in medicine & biology*, vol. 29, no. 7, pp. 1053–1060, 2003.

[15] P. R. Smith, "Ultrasonic phased array techniques using switched-mode excitation," Ph.D. Thesis, University of Leeds, UK, 2013.

[16] D. M. J. Cowell, P. R. Smith, and S. Freear, "Phase-inversion-based selective harmonic elimination (PI-SHE) in multi-level switched-mode tone- and frequency- modulated excitation," *Ultrasonics, Ferroelectrics and Frequency Control, IEEE Transactions on*, vol. 60, no. 6, pp. 1084–1097, 2013.

[17] P. R. Smith, D. M. J. Cowell, B. Raiton, C. V. Ky, and S. Freear, "Ultrasound array transmitter architecture with high timing resolution using embedded phase-locked loops," *Ultrasonics, Ferroelectrics and Frequency Control, IEEE Transactions on*, vol. 59, no. 1, pp. 40–49, 2012.

[18] S. Harput, "Use of chirps in medical ultrasound imaging," Ph.D. Thesis, School of Electronic and Electrical Engineering, University of Leeds, UK, 2012.

[19] D. Wang, Y. Wang, W. Wang, D. Luo, U. Chitgupi, J. Geng, Y. Zhou, L. Wang, J. F. Lovell, and J. Xia, "Deep tissue photoacoustic computed tomography with a fast and compact laser system," *Biomed. Opt. Express*, vol. 8, no. 1, pp. 112–123, Jan 2017. [Online]. Available: http://www.osapublishing.org/boe/abstract.cfm?URI=boe-8-1-112

[20] S. M. Hverven, O. M. H. Rindal, A. Rodriguez-Molares, and A. Austeng, "The influence of speckle statistics on contrast metrics in ultrasound imaging," in *Ultrasonics Symposium (IUS), 2017 IEEE International*. IEEE, 2017, pp. 1–4.